Energy and Buildings 66 (2013) 66–76

Contents lists available at ScienceDirect

Energy and Buildings

journal homepage: www.elsevier.com/locate/enbuild

Predicting the envelope performance of commercial office buildings in Singapore

Chong Zhun Min Adrian*, Wong Nyuk Hien, Ignatius Marcel, Jusuf Steve Kardinal

Department of Building, School of Design and Environment, National University of Singapore, Singapore 117566, Singapore

ARTICLE INFO

Article history:
Received 8 August 2012
Received in revised form 17 June 2013
Accepted 5 July 2013

Keywords:
Urban heat island
Building envelope performance
Window solar heat gain

ABSTRACT

With increasing urbanization today, the negative impact it has on its surroundings is prevalent in many cities and urban areas. Coupled with the need to create and develop sustainable urban developments, it is essential to understand how much the environment as well as its surrounding morphology affects the built environment. Greater emphasis should therefore be placed on urban planning which takes into consideration the surrounding environment and any accompanying effects it might have on the built environment. The integration of design tools with microclimate assessment tools therefore attest to be one with a promising future. This paper presents a methodology for evaluating the building performance of offices in Singapore whilst taking into account its surrounding morphology using GIS as a platform for integration with an urban climatic assessment tool. Hourly weather data which accounts for the urban morphology (input to the model) is obtained by morphing maximum, minimum and average temperature (the output of air prediction model STEVE) into a typical 24 h profile. Good agreement was found between predicted dry-bulb temperatures and measured data. A total of two indicators of envelope performance were used and they are (1) increase in conduction (wall, window and roof) heat gain and (2) solar heat gain through glazing taking into account shading by surrounding buildings and morphology. The model was shown to have good agreement with building energy simulation programme IES-VE©.

1. Introduction

Increased urbanization was found to have a negative impact on the urban environment. The deterioration of the urban environment through urbanization can be seen from a phenomenon known as urban heat island (UHI) [2,3], where an increase building density [1], results in cities recording higher temperatures in comparison to their non-urbanized surroundings.

As a consequence, the distribution of ambient air temperature in an urban canyon, as well as shading provided by surrounding urban morphology would inevitably have an impact on the energy consumption of buildings. Higher temperature also results in greater conduction heat gain through a building's façade while solar shading by neighbouring buildings can reduce fenestration solar gains. Given that a significant amount of energy consumed in a typical commercial building in Singapore is for air conditioning, it is beneficial if the evaluation of an urban environment can be extended to include its impact on buildings.

The objective of this study is therefore to develop a simple methodology that predicts the envelope performance of office buildings in Singapore, taking into account its local urban microclimate. This includes the development of a methodology for morphing the output from urban microclimate models into a complete year of hourly weather data for use as input to the model.

2. Literature review

2.1. Urban climatic mapping

Over recent years, climatic mapping has been increasingly used for urban planning due to its ability to provide a macro overview. Using GIS, different information could be integrated and laid over one another, providing a clearer picture for analysis and comparison.

Using a GIS-based simulation approach, Chen and Ng [4] quantified UHI and wind dynamic characteristics of the urban environment with the use of SVF (sky view factor) and FAD (frontal area density) simulation respectively. These results were then integrated into a climatic map and used to quantify and address concerns on human thermal comfort in an urban environment. Based on a case study of three large housing estates in Hong Kong and regression analysis, the most important variables that have an impact on UHI effect were identified as surface albedo, sky view factor, height to total floor area ratio and altitude [5]. Measurements

* Corresponding author. Tel.: +65 96348653.
E-mail address: bdgczma@nus.edu.sg (C. Zhun Min Adrian).

0378-7788/$ – see front matter © 2013 Elsevier B.V. All rights reserved.
http://dx.doi.org/10.1016/j.enbuild.2013.07.008

Nomenclature

α	absorptance of surface
β	solar altitude angle (°)
δ	solar declination (°)
ε	hemispherical emittance of surface
σ	Stefan Boltzmann constant (W/m^2 K^4)
ρ	ground reflectance
Φ	solar azimuth (°)
Σ	tilt angle (°)
θ	angle of incidence (°)
Ψ	surface azimuth (°)
ω	hour angle
A	surface area (m^2)
AST	apparent solar time (decimal hours)
E_b	beam component of solar radiation incident on surface (W/m^2)
E_d	sky diffuse component of solar radiation incident on surface (W/m^2)
E_r	ground reflected component of solar radiation incident on surface (W/m^2)
ET	equation of time (min)
h_c	coefficient of heat transfer by convection (W/m^2 K)
h_r	coefficient of heat transfer by long-wave radiation (W/m^2 K)
K_d	ratio of diffuse radiation to global radiation
K_T	ratio of global radiation to extraterrestrial radiation
L	latitude (°N, negative in southern hemisphere)
LST	local solar time (decimal hours)
LSTM	longitude of local standard time meridian, °E of Greenwich (negative in western hemisphere)
LON	longitude of site, °E of Greenwich
n	number of days in month m
q	heat transfer rate (W)
SkyEF	sky exposure factor, ratio of exposure to entire sky
T_θ	spectral transmittance of glazing system
N_θ	Inward flowing fraction × spectral absorptance of glazing system
T_e	sol-air temperature (°C)
T_o	outdoor air temperature (°C)
U	U-value (W/m^2 K)
WWR	window wall ratio
ΔR	difference between long-wave radiation incident on surface from sky and surroundings and radiation emitted by blackbody at outdoor air temperature (W/m^2)

Suffix

i	inside surface
o	outside surface
t	hour
d	day
m	month
ms	meteorological station
UHI	with urban heat island effect

conducted by Chen and Wong [6] have also shown that the presence of city parks not only produces a cooling effect at the vegetated areas, but also cools nearby built environment. This was then found to correlate to the reduction of energy consumption within the surrounding buildings with the use of building energy simulation. By overlaying mobile survey measurements and thermal satellite images with land use maps, Jusuf et al. [3] was able to analyze and compare the temperature profiles for different land use. In another study, Katzschner and Mülder [7] utilized GIS to combine land use data, topographical information and climatic data at a regional level. Through GIS, they were able to generate a climate map which contains information on thermal comfort, microclimatic conditions and ventilation patterns. To date however, few have related the impact of microclimatic conditions to building envelope performance at a macro level. Although Kikegawa et al. [8] and Salamanca et al. [9] have integrated building energy models with urban canopy models, these numerical models may be difficult to use for the non-technical user. Furthermore, they may be time-consuming, particularly when evaluating a significantly large area or when the aim is to provide a macro overview of possible development plans.

2.2. Urban morphology and envelope performance

The amount of heat gained or lost through a building's facade is not only dependent on the material construction of the envelope, but also on the ambient conditions surrounding it. Unlike internal conditions (such as setpoint temperature), external conditions are more complicated and may vary depending on the surrounding morphology [3]. A way to quantify the variation in air temperature is through the use of Screening Tool for Estate Environment Evaluation (STEVE). STEVE is an empirical model that calculates the maximum, minimum and average air temperature of a point of interest based on a 50 m radius within an urban area in Singapore. It was developed with the aim to bridge the gap between air temperature prediction models and urban planning. The output of STEVE is based on a regression model that has various urban morphology and climate predictors as independent variables. STEVE was formulated based on data collected over a period of close to 3 years at various locations within the NUS Kent Ridge Campus and One North [10,11]. The independent variables of this model can be divided into two categories as follow:

1. Climate predictors: daily minimum, maximum and average air temperatures; daily average solar radiation (these climate predictors were obtained from the meteorological station).
2. Predictors of urban morphology: percentage of pavement over a 50 m radius; average height to building area ratio; total wall surface area; green plot ratio; sky view factor; and average surface albedo. The green plot ratio is derived using the leaf area index in proportion to the total lot area; the higher the green plot ratio, the denser the greenery condition in a built environment [12].

3. Methodology

3.1. Local outdoor air temperature calculation

Hourly weather data are required as inputs when predicting the performance of a building's enclosure. Hence, to determine the impact of UHI on envelope performance, a method must first be developed for morphing maximum, minimum and average temperature (the output of STEVE) into a 24 h profile.

Temperature measurements were conducted along Shenton Way and Tanjong Pagar in the Central Business District of Singapore (Fig. 1). The equipment used for measurement is the HOBO data logger U12-011 and was housed inside a solar cover to protect it from direct solar radiation. The HOBO U12 has an accuracy of ±0.35 °C for temperatures between 0 °C and 50 °C. Temperatures were recorded at 1 min intervals for a period of approximately two months (March and April 2012). Measured data from March 2012 and April 2012 were compared with temperatures recorded at Singapore's

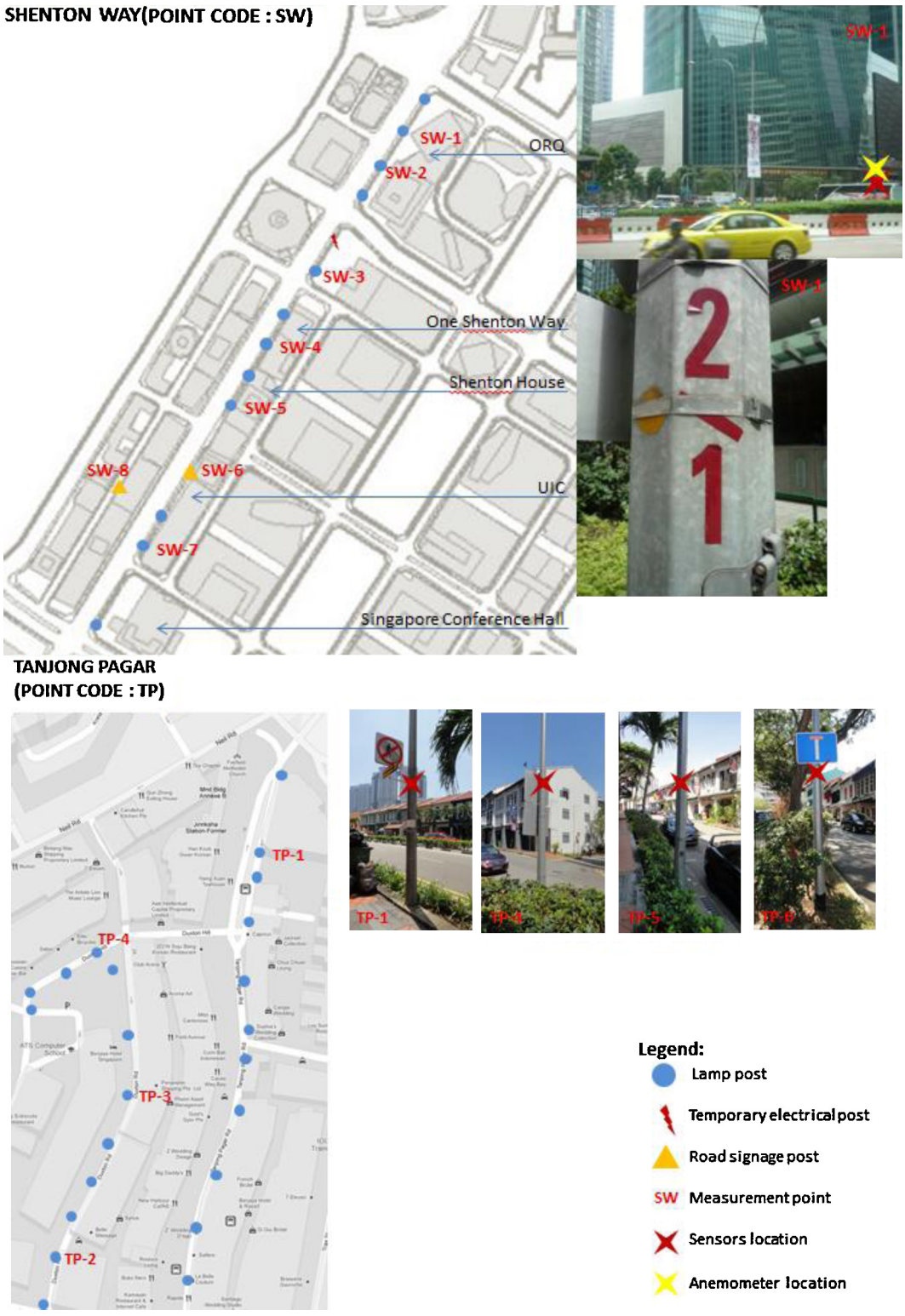

Fig. 1. Measurement points in Central Business District, Singapore.

meteorological station to develop an empirical model (Eqs. (1)–(3)) that is capable of generating a 24 h profile for a typical day in each month within a year. It is important to note that the modified weather data represents typical rather than extreme weather conditions.

$$\text{If } X_t < X_{\text{avg}}, \quad T_t = T_{\min} + (X_t - X_{\min})\left(\frac{a}{b}\right) \tag{1}$$

where $a = (X_{\max} - X_{\min})(T_{\text{avg}} - T_{\min})^2, b = (X_{\text{avg}} - X_{\min})^2(T_{\max} - T_{\min})$

$$\text{If } X_t > X_{\text{avg}}, \quad T_t = T_{\max} - (X_{\max} - X_t)\left(\frac{c}{d}\right) \tag{2}$$

where $c = (X_{\max} - X_{\min})(T_{\max} - T_{\text{avg}})^2, d = (X_{\max} - X_{\text{avg}})^2(T_{\max} - T_{\min})$

$$X_t = (X_t)_m = \left(\frac{1}{n}\right)\sum X_{d,t} \tag{3}$$

n is the number of days in month m and $X_{d,t}$ is air temperature recorded by the meteorological station on day d at hour t. X_t also denoted by $(X_t)_m$ is defined as the variable $X_{d,t}$ averaged over the number of days N for each hour t in month m, generating a 24 h profile of averages. For instance, $(X_1)_2$ represents the average of all air temperatures recorded at Singapore's meteorological station at 1 in the morning in the month of February. X_{min}, X_{avg} and X_{max} represent the average (minimum, average and maximum) temperatures recorded at the meteorological station respectively during month m. X_{min}, X_{avg} and X_{max} were then used as input into STEVE to calculate T_{min}, T_{avg} and T_{max} respectively. These are the average (minimum, average and maximum) temperatures predicted for various points in an urban estate, after considering the surrounding morphology of a building.

Variations in outdoor air temperature with altitude is accounted for using the ICAO Standard Atmosphere [13] and is similar to the temperature model used in EnergyPlus [14]. According to this model, variations in air temperature can be defined as a series of connected segments that are linear in geopotential altitude up to 32 km. Interested readers may refer to ICAO Standard Atmosphere and its reference to EnergyPlus calculations for the detailed formulations.

3.2. Conduction gain through exterior surfaces

Conduction through exterior walls, windows and roof is calculated hourly using the sol-air temperature (Eq. (4)).

$$T_{e,t} = T_{o,t} + \frac{\alpha E_{T,t}}{h_{r,t} + h_c} - \frac{\varepsilon \Delta R}{h_{r,t} + h_c} \quad (4)$$

$$h_{r,t} = 4\varepsilon\sigma\left[\frac{T_{e,t} + T_{o,t}}{2}\right]^3 \quad (5)$$

A linear model for calculating the radiation heat transfer coefficient h_r is used (Eq. (5)). Eqs. (4) and (5) are solved iteratively to determine the sol-air temperature. Values for h_r are calculated hourly to reflect variations with changing air temperatures. External convective coefficient h_c is assumed to be 14 W/m^2 K. To simplify the process, a comparative approach (change in conduction gain) was used to evaluate performance. This difference brought about by UHI is calculated for each external building surface using surface azimuth extracted using GIS. In order to provide a more realistic estimation, results from building energy simulation software IES-VE© would be regressed with the variables in Eq. (6). This would therefore take into account the effect of other factors that may have an effect on conduction gain based on a typical office building in Singapore. This simplification is necessary so that different options or development plans can be considered at a macro scale within a reasonable timeframe, while maintaining sufficient accuracy for an urban planner to make prudent choices.

$$\Delta q_{cond} = a\sum_{\text{month } m=1}\sum_{\text{hour } t=1} nUA(T_{e,t(UHI)} - T_{e,t(ms)}) + C \quad (6)$$

3.3. Calculating incident solar radiation

Incident solar radiation is a required input when calculating the sol-air temperature. The total incident solar radiation is the sum of three components at their respective hour t: the beam component ($E_{b,t}$), the diffuse component from the sky ($E_{d,t}$), and the ground-reflected component ($E_{r,t}$). To calculate these parameters, global solar radiation data which is readily available from the meteorological station is first separated into its direct and diffuse components using Eqs. (10)–(12) [15]. These models have been widely used to separate global radiation into its diffuse and direct components [16,17], and were made applicable to Singapore by Hawlader [15] using measured weather data in comparison with hourly global radiation recorded by the Meteorological Stations in Singapore.

$$E_{b,t} = E_b \cos\theta \quad (7)$$

$$E_{d,t} = E_d \cos^2\left(\frac{\Sigma}{2}\right) \quad (8)$$

$$E_{r,t} = \rho(E_b \sin\beta + E_d)\sin^2\left(\frac{\Sigma}{2}\right) \quad (9)$$

$$(K_d)_t = 1.1389 - 0.9422(K_T)_t - 0.3878(K_T)_{t^2}$$
$$\text{for} \quad 0.225 = (K_T)_t = 0.775 \quad (10)$$

$$(K_d)_t = 0.915 \quad \text{for} \quad 0 = (K_T)_t < 0.225 \quad (11)$$

$$(K_d)_t = 0.215 \quad \text{for} \quad (K_T)_t > 0.775 \quad (12)$$

ρ is the ground reflectance and can be taken to be 0.2 which is typical of surfaces in a city centre [18]. The value of the incident angle θ depends on geographic latitude, surface azimuth, as well as the time of day and year (Eq. (13)). Eqs. (14) and (15) are used to determine the solar altitude β and solar azimuth Φ respectively [18,19]. Surface azimuth Ψ can be defined as the orientation of the building where surfaces facing south is taken as 0°. Surfaces to the west have positive values while those to the east are negative. Using GIS, surface azimuths of different buildings walls in the CBD area was extracted and used to calculate the incident radiation.

$$\cos\theta = \cos\beta\cos(\phi - \Psi)\sin\Sigma + \sin\beta\cos\Sigma \quad (13)$$

$$\sin\beta = \cos L\cos\delta\cos\omega + \sin L\sin\delta \quad (14)$$

$$\cos\Phi = \text{sign}(\omega)\frac{\cos\omega\cos\delta\sin L - \sin\delta\cos L}{\cos\beta} \quad (15)$$

where sign(ω) is +1 when the hour angle is positive and −1 when the hour angle is negative.

In order to evaluate the solar altitude and solar azimuth above, the solar declination δ and hour angle ω was first obtained using Eqs. (16) and (17) [18,19]. The local standard time LST in Singapore was converted to solar time AST using two corrections (Eq. (18)). The first correction accounts for the location of the meteorological station and the meridian on which the local standard time is based. The second correction takes into account the perturbations in the earth's rate of rotation and is accounted for by the equation of time (Eq. (19)).

$$\delta = 23.45\sin(360^\circ \times f) \quad (16)$$

where $f = (284 + n)/365$

$$\omega = 15(\text{AST} - 12) \quad (17)$$

$$\text{AST} = \text{LST} + \frac{\text{ET}}{60} + \frac{\text{LON} - \text{LSTM}}{15} \quad (18)$$

$$\text{ET} = 2.2918(0.0075 + 0.1868\cos B - 3.2077\sin B - 1.4615\cos 2B - 4.089\sin 2B) \quad (19)$$

$$B = \frac{360^\circ(n-1)}{365} \quad (20)$$

3.4. Solar heat gain calculation

Transmitted solar radiation was computed hourly for the entire year and depends on the amount of incident solar radiation. Instead of using normal incidence values to calculate total solar heat gains, transmittance and the inward-flowing fractions are were computed at 10° intervals. This is because spectral property of glazing

varies with angle of incidence. Angular variations in glazing properties are determined using the Fresnel equations [20]. These angular and diffuse transmittance values can be easily calculated from computer programmes such as WINDOW 5.2 [21], or within building energy simulation software IES-VE© using specifications that are usually available from glazing catalogues or ASHRAE handbook fundamentals [18]. Using IES-VE©, the result is a set of solar transmission, absorptance and inward-flowing fraction at 10° intervals. These results were inferred and calculated from normal incidence solar transmission and reflectance of each glazing layer. For simplicity, *g*-value (BFRC) was used to determine the amount of diffuse sky radiation and ground reflected radiation that enters through the glazing. Since most *g*-value or SHGC values provided by manufacturers are normal incidence values, the *g*-values are converted to time-averaged values according to the simplified method used to define *g*-value (BFRC) [22,23]. Eqs. (21) and (22) show how the diffuse and beam solar heat gain are to be calculated respectively. To account for the shading due to surrounding morphology, the beam component is multiplied by the average Sky Exposure Factor (SkyEF) of the building's external surface. SkyEF can be defined as the ratio of the solid angle of the sky patch visible from a certain point on a building's facade to the solid angle of the hemisphere centred at the same point [24]. These ratios are then averaged across the building's external surface. It is multiplied by a factor of 2 because the calculation of SkyEF is based on the ratio of exposure to the entire sky while the ratio of incident direct solar radiation that is not shaded should be based on the ratio from the horizon to the zenith.

$$q_{d,t} = (E_{d,t} + E_{r,t})A(\text{WWR})(g\text{-value}) \quad (21)$$

$$q_{b,t} = (2 \times \text{SkyEF})E_{b,t}A(\text{WWR})(T_{\theta,t} + N_{\theta,t}) \quad (22)$$

Since transmittance and the inward-flowing fractions are determined at ten degree intervals, $T_{\theta,t}$ and $N_{\theta,t}$ were taken as the average of the two spectral values for which the incident angle falls between. For instance, if the angle of incidence falls between 10° and 20° at hour t, $T_{\theta,t}$ would equal to the average spectral transmittance values at 10° and 20°.

3.5. Building energy simulation

For this study, several parameters were varied simultaneously so that the interdependencies between different parameters are accounted for. A total of 25 commercial office buildings around the Central Business District in Singapore were surveyed to provide realistic construction and combinations of envelope components. A detailed investigation into their envelope construction produced 27 different generic envelope combinations (Table 1). Where detailed roof construction was not available, a typical roof construction for office buildings was used. Using IES-VE©, the simulation is modelled based on a typical office building design in Singapore. They were assumed to operate on a 55 h work week, typical of offices in Singapore [25]. Infiltration schedule is the inverse of the cooling schedule because it is assumed that the building is pressurized during operation. Lighting power and ventilation rates were kept at 15 w/m^2 and 0.6 l/s m^2 in accordance to codes of practices of Singapore [26,27]. Two built forms; the pavilion and slab were considered for this study (Fig. 2). The dimensions were determined by keeping a fixed surface area to volume ratio of 0.15 while keeping the height of the building at 10 storeys with a typical storey height of 3.6 m. A ratio of 0.15 was used based on analysis using GIS to extract the volume and corresponding surface area in the CBD area. To determine the possible change in conduction gains brought about by UHI effect, each built form was assumed to be located along the measurement points illustrated in Fig. 1 (SW1–7 and TP1–4). Each model was run twice, once using weather data from the meteorological station and another using temperature measurement conducted along Shenton Way and Tanjong Pagar. The difference was then calculated by subtracting one from the other. The simulations were run from March 2012 to April 2012. Using least squared estimation, this difference was correlated with the independent variables in Eq. (6). This was done for conduction gains through walls, windows and roofs respectively. Eq. (6) was then used to generate a yearly average climatic map which includes the impact of UHI on conduction gains through building enclosures.

The same built forms were used for assessing window solar gain calculations. To determine if the solar gain calculations were sufficiently accurate, they were compared to results generated from the building energy simulation programme IES-VE©. Each form was rotated to account for each of the general orientations (N, NE, E, SE, S, SW, W, and NW). All 27 different generic envelope combinations (Table 1) were simulated and compared to the window solar heat gain model described above.

4. Results and discussion

4.1. 24 h temperature profile

Fig. 3 shows a typical 24 h temperature profile measured along Shenton Way and Tanjong Pagar against the model output described above. From the figure, it can be seen that there is good agreement between predicted and measured data. Agreement between measured and predicted temperature is further illustrated in Figs. 4 and 5. Fig. 4 shows the scatter plot of predicted temperature against what was measured at every data point. It can be seen that the trend line for predicted temperature follows closely that of measured temperature. The scatterplot also illustrates a linear relationship between measured and predicted temperature with a high *R*-squared value of 0.8861. The Pearson's chi-squared test was also used to assess the goodness of fit between measured and predicted data. With 528 data points and a chi-square statistic of 3.18,

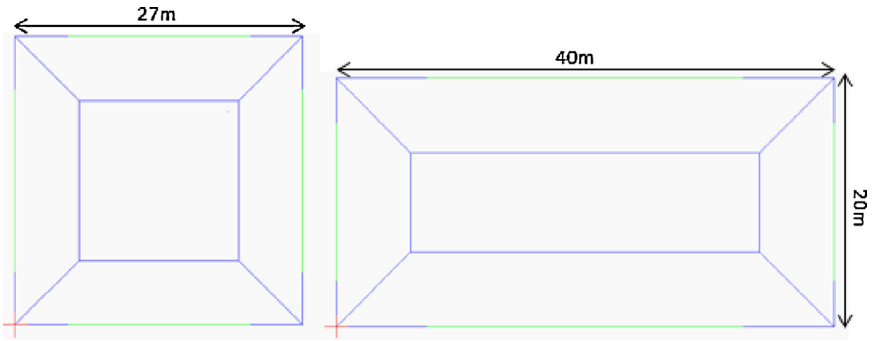

Fig. 2. Plan view of pavilion and slab built form.

Table 1
27 different envelope combination based on survey of buildings around central business district in Singapore.

No.	Wall construction (outside–inside)	Window construction (outside–inside)	Roof construction (outside–inside)	WWR
1	5 mm alum panel, 75 mm insulation, 100 mm air gap, 20 mm plaster board, *U*-value = 0.386	8 mm anti-sun float bronze, 12 mm airspace, 6 mm clear float, *U*-value = 2.930, SC = 0.37	12.5 mm roof gravel, 9.5 mm built up roofing, 50 mm polystyrene insulation, 150 mm concrete slab, 102 mm air layer, 13 mm acoustic tile, *U*-value = 0.637	0.40
2	478 mm glass sheet, 130 mm air gap, 75 mm glass wool, 18 mm plaster gypsum, *U*-value = 0.331	8 mm grey tinted low-E heat strengthened, 12 mm airspace, 8 mm clear heat strengthened, *U*-value = 1.412, SC = 0.29	12 mm tiles, 25 mm screed, 50 mm vermiculite, 50 mm screed, 300 mm concrete, *U*-value = 0.771	0.37
3	30 mm aluminium cladding, 50 mm air gap, 350 mm concrete wall, 20 mm plaster-cement/sand, *U*-value = 1.817	6 mm clear float, 12 mm airspace, 6 mm clear float, *U*-value = 3.005, SC = 0.31	75 mm precast slab, 25 mm polystyrene insulation, 150 mm concrete, *U*-value = 0.862	0.52
4	6 mm single glaze glass, 110 mm air gap, 1.2 mm aluminium back panel, 50 mm rockwool, *U*-value = 0.567	6 mm/12 mm air gap/6 mm double glaze glass, *U*-value = 1.636, SC = 0.27	12.5 mm roof gravel, 9.5 mm built up roofing, 50 mm polystyrene insulation, 150 mm concrete slab, 102 mm air layer, 13 mm acoustic tile, *U*-value = 0.637	0.57
5	6 mm single glaze glass, 70 mm air gap, 1.2 mm aluminium back panel, 50 mm rockwool, 200 mm air gap, 100 mm light weight concrete, 200 mm air gap, 50 mm rockwool, 12 mm gypsum board, 3 mm timber panelling, *U*-value = 0.145	6 mm/12 mm air gap/10 mm double glaze glass, *U*-value = 1.636, SC = 0.38	12.5 mm roof gravel, 9.5 mm built up roofing, 50 mm polystyrene insulation, 150 mm concrete slab, 102 mm air layer, 13 mm acoustic tile, *U*-value = 0.637	0.57
6	8 mm glass, 122 mm air gap, 1.5 mm aluminium backpan, 50 mm rockwool insulation with aluminium foil, *U*-value = 0.390	VRE 19–54 glass (all vision) 6 mm crystal grey, 12 mm air gap, 6 mm clear, *U*-value = 1.50, SC = 0.3	50 mm cement plaster, 50 mm polystyrene, 50 mm cement plaster, 200 mm RC, *U*-value = 0.541	0.58
7	1.2 mm galvanized steel sheet, 50 mm rockwool, *U*-value = 0.626	6 mm tinted glass, 12 mm air gap, 6 mm tinted glass, *U*-value = 1.683, SC = 0.33	12.5 mm roof gravel, 9.5 mm built up roofing, 50 mm polystyrene insulation, 150 mm concrete slab, 102 mm air layer, 13 mm acoustic tile, *U*-value = 0.637	0.53
8	20 mm plaster, 230 mm brickwall, 20 mm plaster, *U*-value = 1.887	6 mm/12 mm air gap/6 mm double glazing, *U*-value = 1.683, SC = 0.33	50 mm cement/sand panel roofing, 50 mm polystyrene insulation, 25 mm cement/sand screed, 130 mm RC slab, *U*-value = 0.547	0.40
9	6 mm glass sheet, 20 mm air gap, 20 mm plaster, 100 mm brickwall, 20 mm plaster, *U*-value = 2.060	6 mm/12 mm air gap/6 mm double glazing, *U*-value = 1.683, SC = 0.33	50 mm cement/sand panel roofing, 50 mm polystyrene insulation, 25 mm cement/sand screed, 130 mm RC slab, *U*-value = 0.547	0.40
10	12 mm plaster, 200 mm brickwall, 12 mm plaster, *U*-value = 2.161	13 mm dark blue laminated, *U*-value = 5.487, SC = 0.9	12.5 mm roof gravel, 9.5 mm built up roofing, 50 mm polystyrene insulation, 150 mm concrete slab, 102 mm air layer, 13 mm acoustic tile, *U*-value = 0.637	0.59
11	20 mm plaster, 200 mm brickwall, 20 mm plaster, *U*-value = 2.618	8 mm tinted heat strengthened glass, *U*-value = 5.632, SC = 0.99	12.5 mm roof gravel, 9.5 mm built up roofing, 50 mm polystyrene insulation, 150 mm concrete slab, 102 mm air layer, 13 mm acoustic tile, *U*-value = 0.637	0.38
12	20 mm plaster, 150 mm brickwall, 20 mm plaster, *U*-value = 2.667	6 mm/12 mm air gap/6 mm bronze tinted low-E, *U*-value = 1.585, SC = 0.33	12.5 mm roof gravel, 9.5 mm built up roofing, 50 mm polystyrene insulation, 150 mm concrete slab, 102 mm air layer, 13 mm acoustic tile, *U*-value = 0.637	0.39
13	4 mm alucobond, 25 mm rockwool insulation, 100 mm space gap, 25 mm aluminium, 40 mm space gap, 25 mm aluminium, 28 mm glass, 25 mm aluminium, *U*-value = 0.517	28 mm Low E double glaze, *U*-value = 1.585, SC = 0.34	50 mm cement/sand screed, 50 mm thermal insulation, waterproof membrane, 25 mm cement/sand screed, 200 mm concrete slab, 12 mm cement skim coat, *U*-value = 0.501	0.65
14	150 mm spandral glass, 1 mm aluminium, air gap, 1 mm aluminium, *U*-value = 1.36	Low-E double glaze, *U*-value = 1.585, SC = 0.32	12.5 mm roof gravel, 9.5 mm built up roofing, 50 mm polystyrene insulation, 150 mm concrete slab, 102 mm air layer, 13 mm acoustic tile, *U*-value = 0.637	0.59
15	30 mm granite, 100 mm air gap, 50 mm mineral wool, 3 mm aluminium lining, *U*-value = 0.618	6 mm/12 mm air gap/6 mm double glazing, *U*-value = 1.683, SC = 0.27	50 mm cement panel, 50 mm polystyrene insulation, 200 mm RC slab, *U*-value = 0.5149	0.54
16	30 mm granite, 70 mm air space, 500 mm concrete, *U*-value = 1.4685	8 mm/8 mm air gap/8 mm double glazzing, *U*-value = 2.02, SC = 0.42	75 mm light weight panel roofing, 50 mm polystyrene insulation, 50 mm cement/sand screed, 150 mm RC slab, *U*-value = 0.528	0.56
17	20 mm cement plaster, 200 mm RC wall, 20 mm cement plaster, *U*-value = 2.606	8 mm clear glass/12 mm air gap/6 mm clear glass, *U*-value = 1.585, SC = 0.28	12.5 mm roof gravel, 9.5 mm built up roofing, 50 mm polystyrene insulation, 150 mm concrete slab, 102 mm air layer, 13 mm acoustic tile, *U*-value = 0.637	0.32
18	19 mm plaster, 115 mm RC wall, 19 mm plaster, *U*-value = 3.504	6 mm tinted double glazed glass, *U*-value = 2.930, SC = 0.26	20 mm waterproofing cement screeding, 75 mm lightweight concrete, 120 mm RC slab, *U*-value = 0.326	0.35
19	3 mm aluminium cladding, 25 mm fibreglass, *U*-value = 1.131	8 mm tinted glass, *U*-value 5.632, SC = 0.42	50 mm cement/sand panel, 1 mm roofing felt, 25 mm polystyrene insulation, 3 mm bituminous membrane, 25 mm cement/sand screed, 150 mm RC slab, *U*-value = 0.883	0.34
20	20 mm plaster, 200 mm RC wall, 20 mm plaster, *U*-value = 2.606	6 mm/12 mm air gap/6 mm double glaze glass, *U*-value = 3.233, SC = 0.38	50 mm cement/sand screed, 50 mm polystyrene insulation, 200 mm RC slab, *U*-value = 0.546	0.30
21	6 mm spandrel, 80 mm air gap, 36 mm insulation, 12 mm gypsum board, *U*-value 0.525	6 mm tinted single glaze, *U*-value = 5.693, SC = 0.48	2.5 mm roof gravel, 9.5 mm built up roofing, 50 mm polystyrene insulation, 150 mm concrete slab, 102 mm air layer, 13 mm acoustic tile, *U*-value = 0.637	0.38

Table 1 (*Continued*)

No.	Wall construction (outside–inside)	Window construction (outside–inside)	Roof construction (outside–inside)	WWR
22	30 mm granite, 45 mm air gap, 125 mm RC wall, 50 mm wood wool slab, 12 mm gypsum board, *U*-value = 1.271	6 mm/12 mm air gap/6 mm double glaze glass, *U*-value = 3.233, SC = 0.42	50 mm cement/sand panel, 50 mm polystyrene board, 25 mm cement/sand screed, 150 mm RC slab, *U*-value = 0.543	0.48
23	30 mm granite, 65 mm air gap, 100 mm RC wall, 10 mm cement plaster, *U*-value = 2.363	6 mm reflective glass/12 mm air gap/6 mm clear glass, *U*-value = 3.233, SC = 0.26	50 mm concrete panel, 50 mm woodwool insulation, 25 mm cement screed, 150 mm RC slab, *U*-value = 1.176	0.26
24	30 mm granite, 50 mm Air gap, 600 mm concrete, *U*-value = 1.355	8 mm/8 mm air gap/8 mm double glazing, *U*-value = 2.889, SC = 0.43	25 mm cement/sand plaster, 25 mm polyurethane insulation foam, 150 mm lightweight concrete, 20 mm cement/sand plaster, *U*-value = 0.621	0.41
25	32 mm Granite, 118 mm air gap, 200 mm brickwall, *U*-value = 1.945	6 mm/12 mm air gap/6 mm tinted double glaze glass, *U*-value = 3.233, SC = 0.28	75 mm precast concrete panel, 50 mm polyurethane insulation foam, 30 mm cement/sand screed, 125 mm RC slab, *U*-value = 0.408	0.34
26	3 mm aluminium cladding, 170 mm air gap, 12 mm gypsum plaster board, 50 mm fibre glass insulation, 12 mm gypsum plaster board, *U*-value = 0.698	6 mm/12 mm air gap/6 mm reflective double glazing, *U*-value = 3.233, SC = 0.30	25 mm waterproof cement, 3 mm motar plas std water, 75 mm lightweight concrete screed, 120 mm RC slab, *U*-value = 0.842	0.45
27	3 mm aluminium panel, 50 mm air gap, 50 mm rock wool, 200 mm air gap, 125 mm brickwall, *U*-value = 0.485	Single glaze, 6.38 mm thick (emilam RB-20), *U*-value = 5.681, SC = 0.45	2.5 mm roof gravel, 9.5 mm built up roofing, 50 mm polystyrene insulation, 150 mm concrete slab, 102 mm air layer, 13 mm acoustic tile, *U*-value = 0.637	0.41

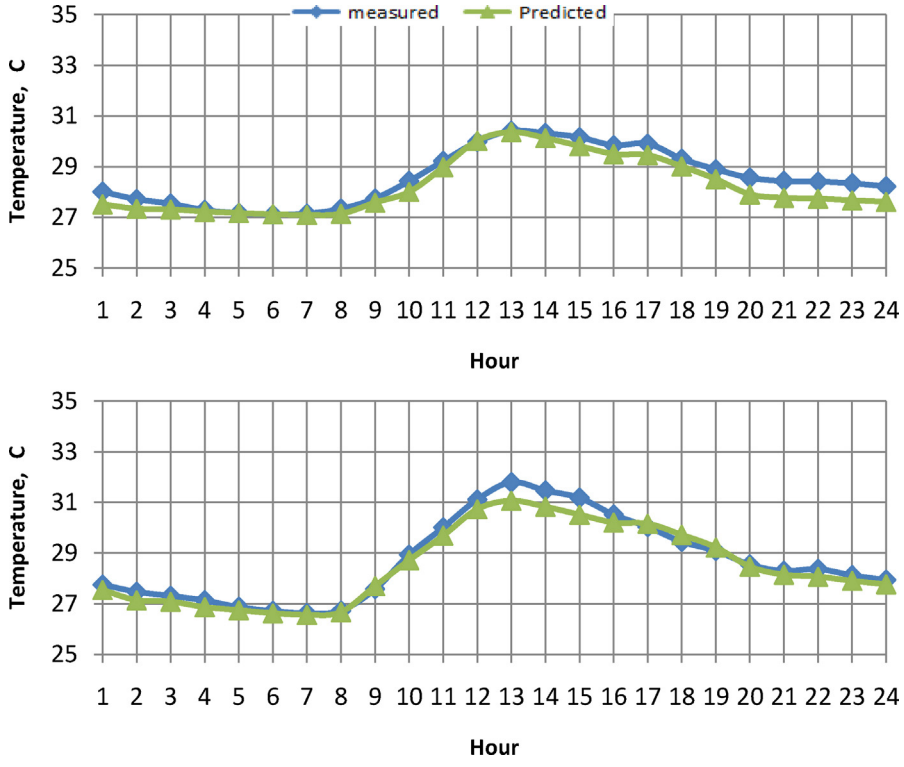

Fig. 3. Typical 24 h temperature profile measured and predicted along Shenton Way (top) and Tanjong Pagar (bottom).

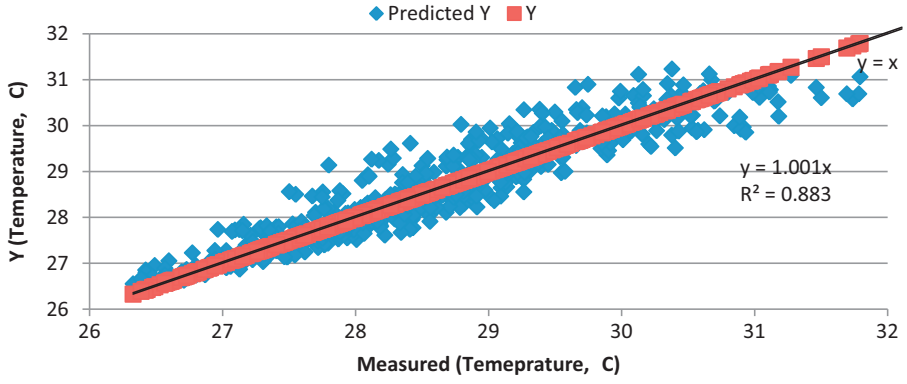

Fig. 4. Measured and predicted temperature against measured temperature for March and April 2012.

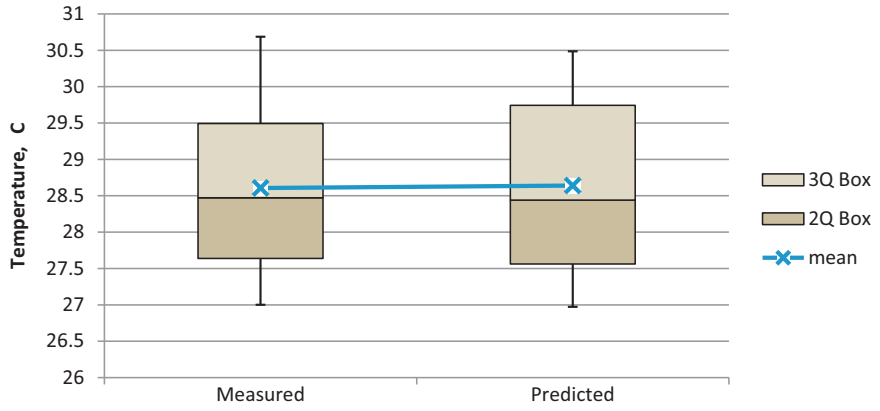

Fig. 5. Box plot showing 3rd quartile, median and 2nd quartile with mean of measured and predicted data. (For interpretation of the references to colour in the text, the reader is referred to the web version of the article.)

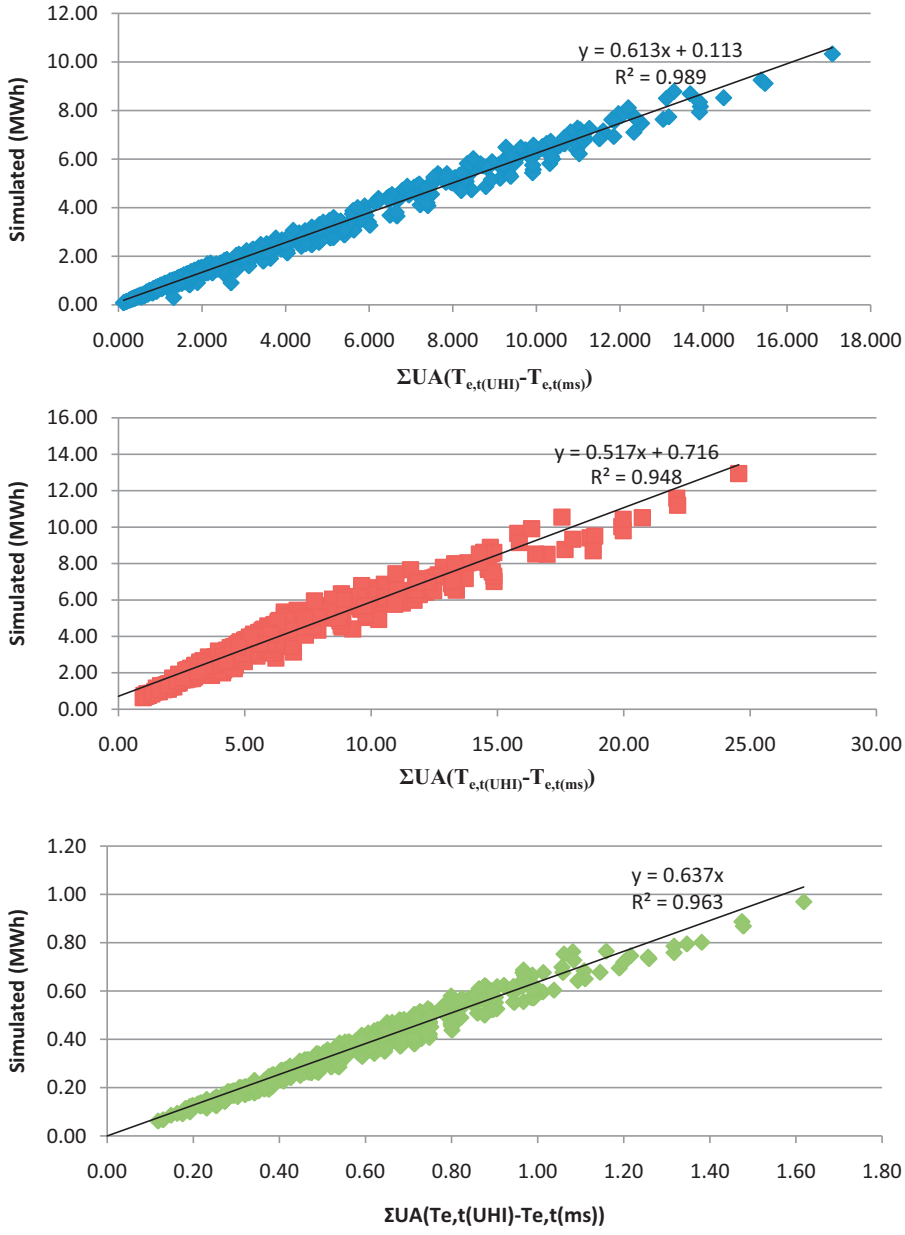

Fig. 6. Simulated results against independent variables used to model conduction gain through opaque wall (top), fenestration (middle) and roof (bottom).

it is obvious that the chi-square statistics do not exceed the lower tail critical value at a 1% significance level. Thus, the null hypothese is not rejected and it can be concluded that there is no significant difference between measured and predicted data.

Fig. 5 is a box and whisker plot based on the average maximum, average minimum and the average 25th, 50th and 75th percentile of measured and predicted temperature. The mean is illustrated with the blue line. From Fig. 4, it can be observed that both predicted and measured data have comparable ranges between both the box (25th and 75th percentile) and between the whiskers (minimum and maximum), with measured data having a slightly higher temperature at maximum (0.2 °C) and the 75th percentile (0.25 °C). The other indicators (minimum, 25th percentile, median and mean) of the box and whisker plot also appears to be similar and without significant difference. Based on these observations, it can be affirmed that the empirical model is able to calculate the typical 24 h profile with sufficient accuracy.

4.2. Change in conduction gains

Fig. 6 shows the scatter plot of the change in heat conducted through the wall, fenestration and roof against their respective *U*-value, area and sol-air temperature. *U*-values were calculated based on the conductivity and thickness of the envelope components provided by the Building and Construction Authority (BCA) Singapore. Based on each respective scatter plot, it can be seen that the possible increase in conduction gain is a linear function of the hypothesized independent variables. This is further affirmed by the high *R*-squared values (0.9895, 0.9513 and 0.9629) of each respective regression models. This fit was obtained with value of h_r that typically varies between 5 and 6 depending on the absorptance of the surface and the respective environmental conditions.

It is important to note that although there is a good fit between predicted and simulated results, the goodness of fit depends a lot on the temperature data through which the model uses as its input. Hence it is important that the urban morphology be accurately accounted for when calculating the 24 h temperature profile for a particular locality.

4.3. Calculating solar heat gain through windows

Fig. 7 shows the glazing solar heat gain calculated using Eqs. (21) and (22) as compared to that obtained using simulation programme IES-VE© for March to April 2012 and May 2012 respectively. It can be seen that the model closely follows the results generated by the building energy simulation programme. Observation of the scatterplot also illustrates a linear relationship between simulated and predicted temperature with a high *R*-squared value of 0.9913 and 0.9882 respectively. The Pearson's chi-squared test was also used to assess the goodness of fit between measured and predicted data. With 286 data points and a chi-square statistic of 42, it can be concluded that the chi-square statistics does not exceed the lower tail critical value at a 1% significance level (70.065 where degree of freedom = 100). Therefore, the null hypothesis is not rejected and it is concluded that there is no significant difference between the predicted and simulated result.

4.4. Application

To provide an overview of an estate's environmental condition as well as the envelope performance of buildings within the estate, the average temperature map is integrated with calculations for conduction gains and solar heat gains. As an illustration, 8 buildings in the CBD area were selected. Using detailed materials construction of each of the building's façade, window solar heat gains and

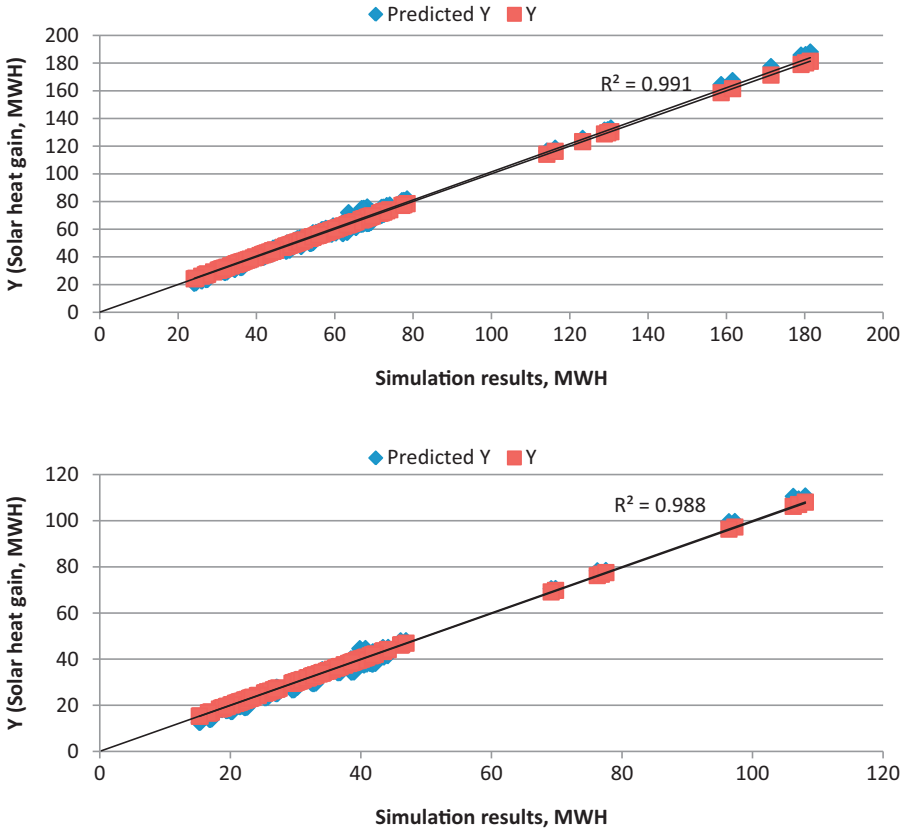

Fig. 7. Simulated and predicted solar gain through glazing against simulation results for March and April 2012 (top) and May 2012 (bottom).

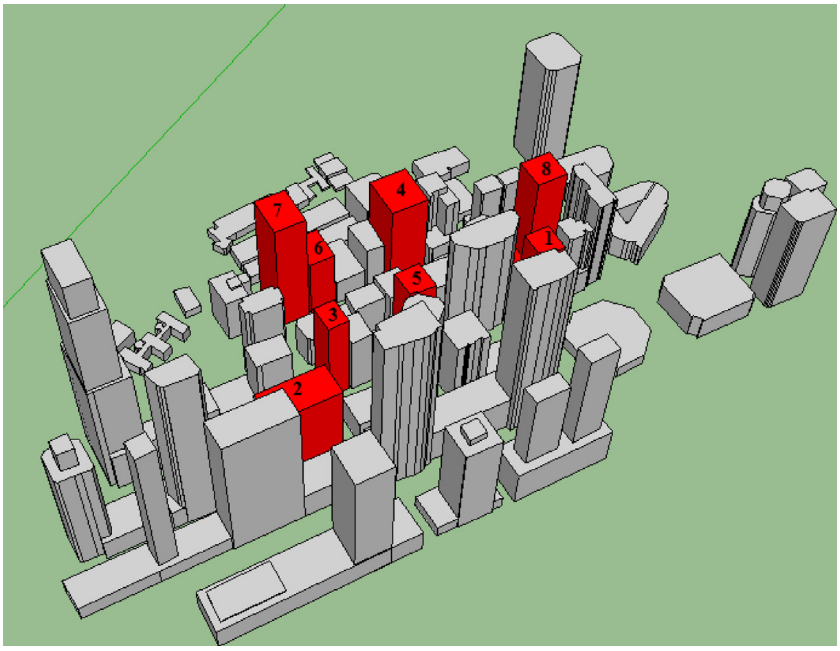

Fig. 8. Model of buildings 1–8 and their surrounding built environment.

the increase in conduction heat gains were calculated. Each surface of every building was calculated separately using exact window and wall areas with surface azimuths extracted from satellite data using GIS. Where data on wall and window areas were not available, they were extracted using GIS. However, if this was to be used for regulating building envelope's performance, it is recommended that exact areas be used for precision. A 3-dimensional model was also used for the calculation of the SkyEF (Fig. 8). The calculated change in conduction gains and solar gains are normalized by dividing their respective envelope area.

Fig. 9 shows the average temperature map integrated with the normalized changes in conduction gain and normalized solar heat gain. Using Fig. 9, buildings that have relatively poor envelope performance are identified as those in red. Since the scale used is a relative one, it also serves to benchmark buildings against one another.

Buildings 5, 6 and 8 have relatively poor performance amongst the 8 buildings when evaluated by the change in conduction gain brought about by UHI, with building 5 performing the worst. Apart from building 8 which has a higher average air temperature, the increase in conduction heat gain at buildings 5 and 6 is most probably due to poor thermal resistance since observation of the temperature map suggests that both buildings are not surrounded by significantly hotter spots. A look into the construction materials of buildings 5 and 6 reveals this observation to be true. The *U*-value (walls and windows) of buildings 5 and 6 yield an average of (2.71 W/m^2 K and 5.8 W/m^2 K) and (2.63 W/m^2 K and 1.6 W/m^2 K) respectively. This is relatively high given that the wall *U*-values of the other buildings generally fall below 1. In addition, the glazing used in building 5 is 8 mm tinted single glaze, thus also contributing to its high conduction gain. It is also important to note that although building 8 is surrounded by higher air temperature due to

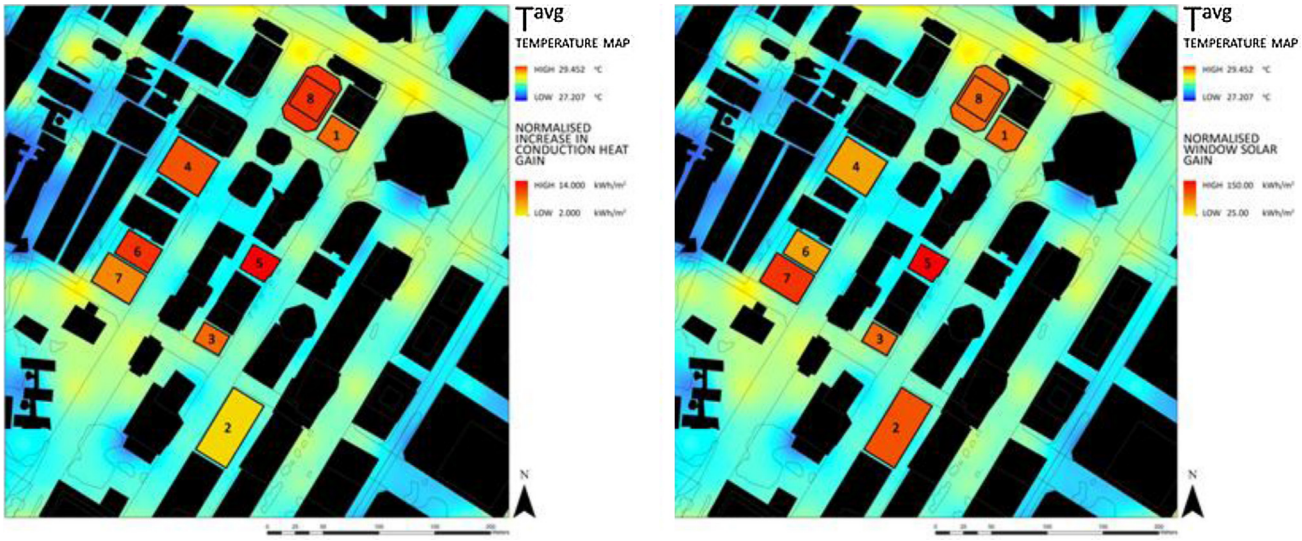

Fig. 9. Normalized increase in conduction heat gain (left) and Normalized window solar heat gain (right). (For interpretation of the references to colour in this figure legend, the reader is referred to the web version of the article.)

its surrounding urban morphology, that is not the sole contributing factor. Its use of single glazing for windows (U-value 5.7 W/m^2 K) have also contributed to its relatively higher increase in conduction heat gain. However, it has an acceptable wall U-value (average 0.67 W/m^2 K) and WWR (approximately 30–40%), which explains its better performance when compared to building 5. When evaluating solar heat gain through glazing, it can be seen that building 5 also has the worst performance, despite being located at a densely built up area which provides significant shading from direct incoming solar radiation. The high solar heat gain can be attributed to the type of glazing used, which in this case is an 8 mm tinted heat strengthened single glaze with a high SHGC of 0.83. Another observation is that although building 6 performed poorly in terms of conduction gains, the amount of solar heat gain through glazing is comparatively acceptable as as identified in yellow in Fig. 9. Hence it is important that buildings be evaluated by both temperature maps, since poor performance in window solar heat gain does not signify the same for conduction heat gain and vice versa. The seperation of conduction gains from solar heat gains also helps in identifying the areas of the building facades that requires the most attention. Besides evaluating current performance, this tool may also be used to determine the effectiveness of different mitigation strategies or developmental plans such as the planting of trees, use of better glazing and implementation of vertical greenery. This however is not within the scope of this paper and would not be elaborated on here.

5. Conclusions

With increasing urbanization and constantly growing urban population, careful planning incorporating the measurement of the environment and any adverse impacts urbanization brings with it should be included. The integration of design tools with microclimate assessment tools therefore attest to be one with a promising future. In this paper, building envelope performance has been integrated with urban climatic assessment using GIS as a platform. Such a tool not only allows urban planners to assess the impact of their designs but also allows authorities to provide a benchmark while taking into consideration the surrounding environment. A total of two indicators of envelope performance were used in this study and they are the increase in conduction (wall, window and roof) heat gain due to the UHI phenomenon, and the solar heat gain through glazing taking into account the effect of shading by surrounding buildings and morphology. Based on observations, it can be seen that conduction gains and solar radiation gains depend on both urban morphology and building materials. Although a low SVF may reduce daytime temperatures via solar shading, the building may still perform poorly if it has low thermal resistance. Hence it is important that planners and building authorities work together to optimize building performance in dense urban areas. This study focuses on the thermal performance of building and further work includes investigation of daylight potential and thermal comfort. With greater emphasis on sustainable urban development, the prospect of an effective urban climatic tool lies in its ability to analyze and evaluate the interaction between buildings and their surrounding morphology. Providing a macro overview of different developmental plans combined with different performance indices therefore not only provides urban planners with the ability to make informed planning decisions, but also provides a platform for regulating building energy consumption which has been shown to be significant [28].

References

[1] M. Santamouris, D.N. Asimakopoulos, V.D. Assimakopoulos, N. Chrisomallidou, N. Klitsikas, D. Mangold, A. Tsangrassoulis, Energy and Climate in the Urban Built Environment, James & James, London, UK, 2001.
[2] T.R. Oke, The energetic basis of the Urban Heat Island, Quarterly Journal of the Royal Meteorological Society 108 (1982) 1–24.
[3] S.K. Jusuf, N.H. Wong, E. Hagen, R. Anggoro, H. Yan, The influence of land use on the urban heat island in Singapore, Habitat International 31 (2007) 232–242.
[4] L. Chen, E. Ng, Quantitative urban climate mapping based on a geographical database: a simulation approach using Hong Kong as a case study, International Journal of Applied Earth Observation and Geoinformation 13 (4) (2011) 586–594.
[5] R. Giridharan, S. Ganesan, S. Lau, Daytime urban heat island effect in high-rise and high-density residential developments in Hong Kong, Energy and Buildings 36 (6) (2004) 525–534.
[6] Y. Chen, N.H. Wong, Thermal benefits of city parks, Energy and Buildings 38 (2) (2006) 105–120.
[7] L. Katzschner, J. Mülder, Regional climatic mapping as a tool for sustainable development, Journal of environmental management 87 (2008) 262–267.
[8] Y. Kikegawa, Y. Genchi, H. Yoshikado, H. Kondo, Development of a numerical simulation system for comprehensive assessments of urban warming countermeasures including their impacts upon the urban building's energy-demands, Applied Energy 76 (2003) 449–466.
[9] F. Salamanca, A. Krpo, A. Martilli, A. Clappier, A new building energy model coupled with an urban canopy parmeterization for urban climate simulations – Part 1. Formulation, verification, and sensitivity analysis of the model, Theoretical and Applied Climatology 99 (2009) 331–344.
[10] N.H. Wong, S.K. Jusuf, An assessment method for existing greenery conditions in a university campus, Architectural Science Review 51 (3) (2008) 116–126.
[11] N.H. Wong, S.K. Jusuf, GIS-based greenery evaluation on campus master plan, Landscape and Urban Planning 84 (2008) 166–182.
[12] B.L. Ong, Green plot ratio: an ecological measure for architecture and urban planning, Lansdcape and Urban Planning 63 (2003) 197–211.
[13] ICAO Standard Atmosphere, Manual of the ICAO Standard Atmosphere Extended to 32 kilometres (105,000 feet), International Civil Aviation Organization, Montreal, 1964.
[14] UIUC, LBNL, EnergyPlus Engineering Reference: The Reference: to EnergyPlus Calculations, 2011.
[15] M.N.A. Hawlader, Diffuse, global and extra, terrestrial solar radiation for Singapore, International Journal of Ambient Energy 5 (1) (1984) 31–38.
[16] B.Y.H. Liu, R.C. Jordan, The interrelationship and characteristic distribution of direct, diffuse and total solar radiation, Solar Energy 4 (1960) 1–19.
[17] D.W. Ruth, R.E. Chant, The relationship of diffuse radiation to total radiation in Canada, Solar Energy 18 (2) (1976) 153–154.
[18] ASHRAE, ASHRAE Handbook, 2009: Fundamentals, American Society of Heating Refrigerating and Air-Conditioning Engineers, Atlanta, GA, 2009.
[19] J.A. Duffie, W.A. Beckman, Solar Engineering of Thermal Processes, John Wiley and Sons, New York, 2006.
[20] IES, ApacheSim Calculation Methods (Virtual Environment 6.3).
[21] LBL, WINDOW 5.2: A PC Program for Analyzing Window Thermal Performance for Fenestration Products. LBL-44789, Lawrence Berkeley Laboratory, Berkeley, 2003.
[22] IES, Constructions Database User Guide: Virtual Environment 5.9.
[23] BFRC, BFRC Guidance Note.
[24] Z. Ji, C.K. Heng, L.C. Malone-Lee, D.J.C. Hii, P. Janssen, K.S. Leung, B.K. Tan, Evaluating environmental implications of density: a comparative case study on the relationship between density, urban block typology and sky exposure, Automation in Construction 22 (2011) 90–101.
[25] S.E. Lee, W. Schafer, H.S. Majid, Energy Performance Assessment and Classification of Commercial Buildings in Singapore (Report No. NUS Project No: R-296-0056-490/R-296-0056-592), National University of Singapore, Central of Total Building Performance, Singapore, 2004.
[26] SPRING, Singapore Standard SS 531: Code of Practice for Lighting of Work Places Part 1: Indoor, SPRING Singapore, Singapore, 2006.
[27] SPRING, Singapore Standard SS 553: Code of Practice for Air-Conditioning and Mechanical Ventilation in Buildings, SPRING Singapore, Singapore, 2009.
[28] WBCSD, Energy Efficiency in Buildings.